Spontaneous Symmetry Breaking in Two Coupled Nanomechanical Electron Shuttles

Chulki Kim, Jonghoo Park, and Robert H. Blick*

University of Wisconsin-Madison, Electrical & Computer Engineering, 1415 Engineering Drive, Madison, Wisconsin 53706, USA

(Received 31 March 2010; published 4 August 2010)

We present spontaneous symmetry breaking in a nanoscale version of a setup prolific in classical mechanics: two coupled nanomechanical pendula. The two pendula are electron shuttles fabricated as nanopillars [D. V. Scheible and R. H. Blick, Appl. Phys. Lett. **84**, 4632 (2004).] and placed between two capacitor plates in a homogeneous electric field. Instead of being mechanically coupled through a spring they exchange electrons, i.e., they shuttle electrons from the source to the drain "capacitor plate." The nonzero dc current through this system by external ac excitation is caused via dynamical symmetry breaking. This symmetry-broken current appears at sub- and superharmonics of the fundamental mode of the coupled system.

DOI: 10.1103/PhysRevLett.105.067204 PACS numbers: 85.85.+j, 45.80.+r

Spontaneous symmetry breaking is one of the fundamental ideas in elementary particle physics when unified gauge field theories are applied [1], e.g., breaking the gauge symmetry leads to the difference in the electromagnetic and the weak interaction. Commonly, one refers to a classical mechanics example to visualize symmetry breaking, such as a thin bar under pressure from both its clamping points. Obviously, the equations of motion are invariant around the symmetry axis along the beam. Once the force reaches a critical level the compressed bar will buckle and thus break the initial symmetry. Although, in the buckled state the bar will be in an energetic minimum, the symmetry of this configuration is reduced. From a quantum mechanical point of view the key question is into which of the many degenerate energetic minima the compressed bar will collapse to and what kind of fluctuation will have caused this transition. Naturally, for a large bar governed by classical mechanics it would be hard to associate the buckling with quantum mechanical states. The situation changes drastically when one considers quantum electromechanical systems [2], such as buckled nanomechanical beams which have been theoretically discussed by Carr *et al.* [3]. In other words nanomechanical devices have the potential to address fundamental quantum mechanics [4–7].

In the following we will present electron transport measurements via two coupled electron shuttles at room temperature under ac or dc excitation. The two shuttles we fabricated have the same physical dimensions, are isolated from ground, and possess metallic tips. The actual realization of the device is shown in the scanning electron microscope graph in Fig. 1(a): the two nanopillars forming the shuttles are placed in series between source and drain contacts. The diameters of the islands on top of each nanopillar is 65 nm with pillar heights of 250 nm. The interpillar distance is 17 nm and is much less than the gaps to source and drain, enhancing mode coupling. The distance from source to the first pillar and drain to the second one are identical, making the setup indeed very symmetric. Our particular focus will be on how breaking the local symmetry leads to the rectified current as recently conjectured by Ahn *et al.* [8]. The fundamental outcome is that although both the nanomechanical and the nanoelectronic circuits are operated in the linear regimes an ac voltage can be rectified. Commonly, rectification only occurs based on a nonlinearity, however, such symmetry breaking in coupled nanomechanical pendula is exactly what is predicted in Ref. [8].

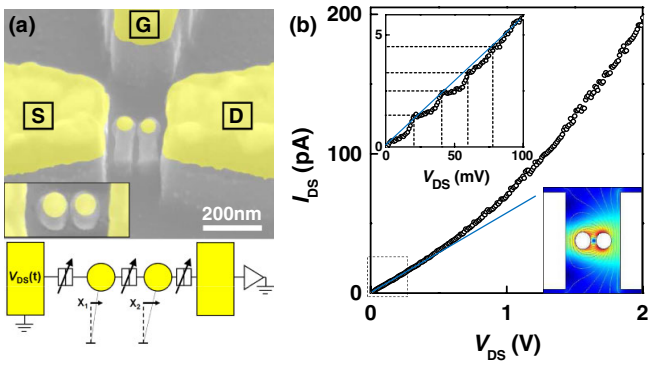

FIG. 1 (color online). (a) Aerial view in a scanning electron microscope of two coupled electron shuttles. The two nanopillars' gold tops have diameters of ≅65 nm with a total nanopillar height of around 250 nm. The inset gives a top view of the coupled nano-electromechanical pendula. The scale bars are 200 nm in both graphs. Below: Sketch of the measurement setup. An applied ac and dc bias voltage (V_{DS}) displaces the two pendula by x_1, x_2 and the resulting current I_{DS} is amplified. (b) Direct current I_{DS} vs bias voltage V_{DS} in the case of pure self-excitation, i.e., $V_{ac} = 0$ at room temperature. The upper inset shows low bias regime with the dashed lines indicating the occurrence of Coulomb charging effects (see text for details). The lower inset gives a finite-element simulation of the electric field distribution under an applied bias voltage (top view). The field intensity is maximal between the two pillars.

The two nanopillars are milled out of a silicon-on-insulator (SOI) material, where the top crystalline silicon is 190 nm thin and the insulating SiO_2 is about 350 nm thick. A 50 nm top gold layer serves as the electrical conduction path. The deposited metal serves as an etch mask in a dry etch step which mills out the SOI material around the pillars. We apply a CF_4 plasma etch step and etch into the SiO_2 insulating layer, thus ensuring electron transport via the metallic islands (further processing details are given in Ref. [9]). The nanoscale circuit is placed in an impedance matched transmission line in order to minimize signal loss along the line. All measurements are performed under vacuum in a probe station at room temperature. The station is placed in a Faraday cage and is equipped with radio frequency contact probes covering the range from dc to 50 GHz (a bias-tee allows ac or dc superposition with high precision). The equivalent circuit diagram is given in the lower part of Fig. 1(a): the two pillars can be individually displaced by x_1 and x_2, which lead to tunable resistances and capacitances (arrow boxes).

In the first measurement we trace the direct current at different voltage bias values at room temperature as shown in Fig. 1(b). At first glance the IV characteristic appears to be linear with only a small deviation ($\propto V^2$) at above 1 V. Electron shuttling leads to the nonzero current, which is caused by self-excitation as we have shown earlier for single nanopillars [10]. This can also be shown for lateral electron shuttles [11,12]. In this particular case we assume that several mechanical modes of the coupled nanopillars (see below in Fig. 2) support the current. The ease of excitation is supported by the finite-element numerical simulation shown in the inset of Fig. 1(b). Obviously, the electric field intensity is dramatically enhanced around the two pillars, enabling the onset of mechanical oscillations under an applied dc bias voltage. Closer inspection of the low-voltage regime reveals the onset of Coulomb blockade (CB) in these serially coupled electron shuttles, as predicted by Gorelik *et al.* [13]. The dashed lines in the inset indicate the individual Coulomb staircase, which is getting weaker towards voltages above 100 mV. A brief investigation of the trace reveals that the CB charging energy is of the order of the room temperature energy at 26 meV. Since we are operating the coupled shuttles at large ac-voltage swings ($>$100 mV amplitude) as compared to the thermal background ($V_{\mathrm{th}} \cong 26$ mV), we can focus on the overall linear IV characteristic. For all measurements presented here the gate voltage potential was left at ground.

A radio frequency signal in the range of 1 MHz to 1 GHz is applied via high-frequency probes in order to trace the mechanical spectrum of the coupled nanopillars, similar to earlier work on single nanopillars [9,11]. The resulting output current from the coupled electron shuttles is a time-averaged dc signal leading to the spectrum shown in Fig. 2. The dc response of the coupled shuttles to the ac excitation is plotted at a dc bias voltage of $V_{\mathrm{DS}} = 0$ mV. A

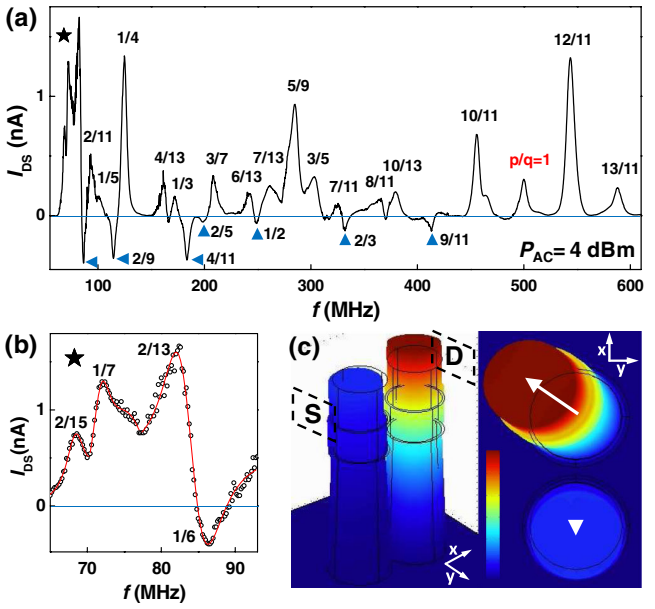

FIG. 2 (color online). (a) Spectrum of drain current I_{DS} vs f the excitation frequency of the coupled nanopillars. The current resonances are labeled according to the commensurate mode numbers p/q where the fundamental mode is found to be at $\omega_o/(2\pi) = 504$ MHz from finite-element simulations. The externally applied power of the radio frequency source was $P =$ 4 dBm. Note the seven distinct current peaks in the reverse current (blue triangles). This electromechanical pumping mechanism pushes electrons against the dc bias of $V_{\mathrm{DS}} = 0$ mV. The low-frequency region ($\star$) is plotted in detail in (b). The red (light gray) line indicates fits to the resonances taking into account different line shapes. (c) Finite-element simulation based on COMSOL showing the fundamental mode of the coupled pendula in a 3D (left) and top view (right). The color coding indicates the displacement within the nanopillars.

broad set of resonances can be identified representing different modes of the coupled nanopillars. On closer inspection of the overall spectrum we find that the multitude of peaks arises due to a parametric instability caused by dynamical symmetry breaking, as predicted by Ahn *et al.* [8]. Once a particular mode is selected among possible mechanical modes, the initial symmetry (no net current) is broken and electrons are shuttled from source to drain. Altering the external perturbation (ac-voltage excitation at a particular frequency) then leads to the selection of different modes. The ratios noted at each peak follow $(p/q)\omega_0/(2\pi)$ with p, q being integers. From finite-element simulations we find that the most likely fundamental mode of the coupled nanopillars is at around $\omega_o/(2\pi) = 504$ MHz at $p/q = 1$, see Fig. 2(a). Most of the corresponding frequencies with the given integer combinations are accurate in the range of ± 3 MHz with four resonances being off by ± 7 MHz. Unlike the theoretical prediction [8], we find both even and odd numbers for q. The hierarchy of resonances is also slightly different from the theoretical result in that the current spectrum of the

coupled electron shuttles has a richer structure with higher orders for p. We can attribute these differences to more degrees of freedom in the real device allowing mechanical modes in all three spatial dimensions.

With increasing external ac power we observe peak broadening, overlapping with neighboring peaks. We find the modes with the winding numbers, p/q generated by ''Farey sums'' of neighboring modes' fractions when overlapping on the left and right: The numerator is the sum of the numerators of the fractions on either side, and the denominator is the sum of the denominators of the fractions on either side [14]. For instance, $p/q = 1/7 = (2 + 2)/(15 + 13)$, $2/13 = (1 + 1)/(7 + 6)$, $2/11 = (1 + 1)/(6 + 5)$ and so on. A similar behavior was observed in nonlinear systems showing a structure of Arnold tongues [15]. The appearance of fractions of the fundamental mode and Farey trees with neighboring modes' fractions indicate that we detect dynamical symmetry breaking.

Most peaks of the spectrum show a forward current, as one expects under forward bias, while some of the peaks give a reverse current (blue triangles). This remarkable feature of the coupled shuttles, i.e., reverse shuttling or pumping, marks a bistability depending on initial conditions, such as positions and velocities of two islands at a given time. We need to note, as will be underlined theoretically below, that the resulting rectified current at zero bias observed here is solely due to a dynamical symmetry breaking and not by a mechanical or electronic nonlinearity. The resonance shapes of the two-nanopillar system are analyzed in Fig. 2(b) in detail: a magnified part of the spectrum at below 100 MHz is shown with three fits (red [light gray] line) indicating the different line shapes. The resonance around 69 MHz follows the conventional Lorentzian, while the trace at 84 MHz shows a maximum and minimum.

We now turn to the details of the rectification effect due to symmetry breaking: as an example we select the pronounced resonance at $(13/11)\omega_0$. The particular peak around 589 MHz is plotted in Fig. 3(a) and marked as δ. The off-resonance background is labeled with η. In Fig. 3(b) the IV traces for these two frequency points are given: as expected for the background the η line shows a linear dependence crossing through the origin of the graph. A small offset in the η trace results from the superimposed ac excitation voltage. In contrast the δ trace reveals a clear offset under finite ac excitation at 589 MHz. This motion of the coupled charge shuttle indicates the existence of a bifurcation point [8].

The theoretical underpinning for this bifurcation of the coupled shuttle leads to the rectified current [8]. A sinusoidal electromagnetic excitation $V_0 \sin(\omega t)$ is applied to the source contact, inducing mechanical displacement of the shuttle at their eigenfrequencies. We can assume that the capacitances between the electrodes are constant, while

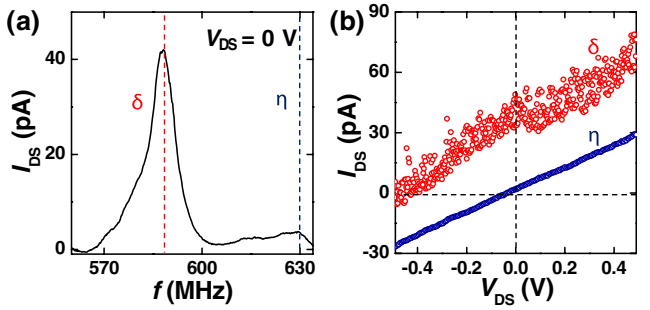

FIG. 3 (color online). (a) Current response on and off resonance: at 589 MHz (δ) with an ac radio frequency excitation of -3 dBm a strong mechanical response of the coupled pendula is obtained, while at off resonance (η) only a weak current shows. (b) Bias dependence of the coupled nanopillars on resonance δ and off resonance η. While we find an ohmic response for both cases the red (light gray) δ trace is offset from the blue (dark gray) η trace. This offset results from the rectification through the coupled nanomechanical shuttles.

the tunneling resistance R varies with electrode distance as $R_1(x_1) = R_1(0)e^{x_1/\lambda}$, $R_2(x_1 - x_2) = R_2(0)e^{(x_2-x_1)/\lambda}$, $R_3(x_2) = R_3(0)e^{-x_2/\lambda}$, where λ is the tunneling length. The x_j refer to the three junctions ($j = 1, 2, 3$) in series, i.e., from source to the first nanopillar, in between the pillars, and finally from the second pillar towards drain. In the following we consider a symmetric configuration: $c_1 = c_3 = 2c_2 \equiv c$ and $R_1(0) = 0.5R_2(0) = R_3(0) \equiv R$. The coupled nanopillars can be assumed to show a *linear* response under modest excitation, as measured in Fig. 1(b), leading to a mechanical displacement, which can be described by a differential equation in the adiabatic limit ($\omega_0 Rc \ll 1$) [8]

$$\ddot{x} + \gamma\dot{x} + \omega_0^2 x = -\frac{cV_0^2 \sin\omega t}{mL} \tanh\left[\frac{3x}{4\lambda}\right], \qquad (1)$$

where $x = x_1 - x_2$ is the relative coordinate, γ, ω_0 and m denote the friction coefficient, the natural angular frequency of the shuttles and the nanopillar's mass in a symmetric configuration and L is the source-drain distance. There is a pair of bistable solutions, $x(t)$ and $-x(t)$. The time-averaged direct current is found to be

$$I_{\mathrm{dc}} = \frac{\omega V_0}{4\pi R} \int_{t_0}^{t_0+2\pi/\omega} \frac{\sin\omega t}{e^{x(t)/2\lambda} + e^{-x(t)/\lambda}} dt. \qquad (2)$$

For a single nanopillar with a symmetric source drain the direct current with ac input voltage will always average out to zero in a similar calculation to above. However, for two coupled nanopillars the symmetry will be broken leading to a dc signal, as we observe in Fig. 3(b). We note that this current only can be found for two coupled nanopillars.

In order to further verify the dynamical symmetry breaking and the resulting rectification we determined the ac-power dependence of the low-frequency end at around 80 MHz, revealing the expected Arnold tongues [16].

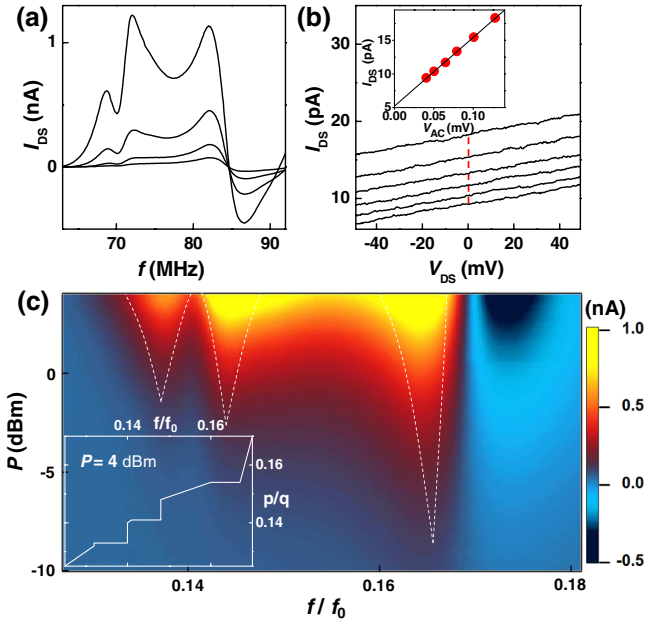

FIG. 4 (color online). Arnold tongues: (a) mechanical resonances at around 80 MHz under increased ac power. (b) The dc bias dependence with gradually increased ac-power, from −20 dBm (bottom) to −15 dBm (top). Inset shows the linear dependence of the rectified direct current upon increasing ac-power. (c) Color scale plot of the total power dependence, revealing Arnold's tongues with the whited dashed lines being guides to the eye. Inset shows a devil's staircase plot depicting the width of each bistable region.

Figure 4(a) shows the detailed power dependence of the output current with line plots with the power level increasing from −10 dBm to +4 dBm. In Fig. 4(b) the maximal current at 83 MHz is plotted vs dc bias and ac power ramped up as the parameter. The inset gives the scaling of generated direct current with respect to applied ac power, indicating the rectification. In Fig. 4(c), finally, the total power dependence is shown in a color scale plot: the boundaries of each tongue are seen. The experimental bifurcation diagram shows the gradual appearance of higher order resonances as the input power increases. The thin dashed lines trace the increase in width as expected for Arnold's tongues. The appearance of Arnold's tongues is also observed in mathematical simulations of two charge shuttles coupled via electron tunneling as discussed in Ref. [8]. In each bistable region the fundamental mode and the external excitation are mode locked in spite of the frequency mismatch. A devil's staircase depicts winding numbers of the mode-locked regions, as shown in the inset of Fig. 4(c). This staircase maps the widths of the Arnold's tongues, defined as the FWHM for a given power of ac excitation. Even though this two pillar system does not have a perfect left-right symmetry, driving the enhanced net current was possible due to the robustness of the observed mode locking.

In summary we detected a rectified dc signal via symmetry breaking in a coupled electron shuttle under the application of an ac voltage. Identified resonances were associated with the fundamental mode of the system within a theoretical framework [8]. Arnold tongues were revealed when the ac power is increased. Each tongue shows the symmetry-broken current in which the system is mode locked with the external ac driving voltage. This setup has potential as a bifurcation amplifier for signal processing applications [17] and can prove to be useful for energy scavenging applications [18].

The authors like to thank DARPA for support through the NEMS-CMOS & CSAC programs (N66001-07-1-2046) and the Graduate School of the University of Wisconsin-Madison for support through a Draper-TIF grant. C. K. would like to thank K. H. Ahn for very helpful discussions.

*blick@engr.wisc.edu

[1] S. Weinberg, Rev. Mod. Phys. **46**, 255 (1974).
[2] M. Blencowe, Phys. Rep. **395**, 159 (2004).
[3] S. M. Carr, W. E. Lawrence, and M. N. Wybourne, Phys. Rev. B **64**, 220101(R) (2001).
[4] H. G. Craighead, Science **290**, 1532 (2000).
[5] C. H. Metzger and K. Karrai, Nature (London) **432**, 1002 (2004).
[6] A. Naik *et al.*, Nature (London) **443**, 193 (2006).
[7] G. A. Steele *et al.*, Science **325**, 1103 (2009).
[8] K. H. Ahn, H. C. Park, J. Wiersig, and J. Hong, Phys. Rev. Lett. **97**, 216804 (2006).
[9] H. S. Kim, H. Qin, and R. H. Blick, Appl. Phys. Lett. **91**, 143101 (2007).
[10] H. S. Kim, H. Qin, and R. H. Blick, New J. Phys. (to be published).
[11] D. V. Scheible and R. H. Blick, Appl. Phys. Lett. **84**, 4632 (2004).
[12] D. R. Koenig, E. M. Weig, and J. P. Kotthaus, Nature Nanotech. **3**, 482 (2008).
[13] L. Y. Gorelik *et al.*, Phys. Rev. Lett. **80**, 4526 (1998).
[14] P. Cvitanović, M. H. Jensen, L. P. Kadanoff, and I. Procaccia, Phys. Rev. Lett. **55**, 343 (1985).
[15] J. A. Glazier, M. H. Jensen, A. Libchaber, and J. Stavans, Phys. Rev. A **34**, 1621 (1986).
[16] S.-B. Shim, M. Imboden, and P. Mohanty, Science **316**, 95 (2007).
[17] R. Almog, S. Zaitsev, O. Shtempluck, and E. Buks, Phys. Rev. Lett. **98**, 078103 (2007).
[18] J. A. Hagerty, F. B. Helmbrecht, W. H. McCalpin, R. Zane, and Z. B. Popovic, IEEE Trans. Microwave Theory Tech. **52**, 1014 (2004).